Title

Charged-Iron-Particles Found in Galactic Cosmic Rays are Potent Inducers of Epithelial Ovarian Tumors

Journal

Radiation Research, 190(2)

ISSN

0033-7587

Authors

Mishra, Birendra
Lawson, Gregory W
Ripperdan, Ryan
et al.

Publication Date

2018-08-01

DOI

10.1667/rr15028.1

Peer reviewed

HHS Public Access

Author manuscript

Radiat Res. Author manuscript; available in PMC 2019 August 01.

Published in final edited form as:

Radiat Res. 2018 August ; 190(2): 142–150. doi:10.1667/RR15028.1.

Charged-Iron-Particles Found in Galactic Cosmic Rays are Potent Inducers of Epithelial Ovarian Tumors

Birendra Mishra[a,d], **Gregory W. Lawson**[e], **Ryan Ripperdan**[a], **Laura Ortiz**[a], and **Ulrike Luderer**[a,b,c,1]

[a]Department of Medicine, University of California Irvine, Irvine, California 92617

[b]Department of Developmental and Cell Biology, University of California Irvine, Irvine, California 92617

[c]Program in Public Health, University of California Irvine, Irvine, California 92617

[d]Department of Human Nutrition, Food and Animal Sciences, University of Hawaii at Manoa, Honolulu, Hawaii 96822

[e]Office for Laboratory Animal Care, University of California Berkeley, Berkeley, California 94720-7150

Abstract

Astronauts traveling in deep space are exposed to high-charge and energy (HZE) particles from galactic cosmic rays. We have previously determined that irradiation of adult female mice with iron HZE particles induces DNA double-strand breaks, oxidative damage and apoptosis in ovarian follicles, causing premature ovarian failure. These effects occur at lower doses than with conventional photon irradiation. Ovarian failure with resultant loss of negative feedback and elevated levels of gonadotropin hormones is thought to play a role in the pathophysiology of ovarian cancer. Therefore, we hypothesized that charged-iron-particle irradiation induces ovarian tumorigenesis in mice. In this study, three-month-old female mice were exposed to 0 cGy (sham) or 50 cGy iron ions and aged to 18 months. The 50 cGy irradiated mice had increased weight gain with age and lack of estrous cycling, consistent with ovarian failure. A total of 47% and 7% of mice irradiated with 50 cGy had unilateral and bilateral ovarian tumors, respectively, whereas 14% of mice in the 0 cGy group had unilateral tumors. The tumors contained multiple tubular structures, which were lined with cells positive for the epithelial marker cytokeratin, and had few proliferating cells. In some tumors, packets of cells between the tubular structures were immunopositive for the granulosa cell marker FOXL2. Based on these findings, tumors were diagnosed as tubular adenomas or mixed tubular adenoma/granulosa cell tumors. In conclusion, charged-iron-particle-radiation induces ovarian tumors in mice, raising concerns about ovarian tumors as late sequelae of deep space travel in female astronauts.

[1]Address for correspondence: Center for Occupational and Environmental Health, 100 Theory Drive, Suite 100, Irvine, CA 92617; uluderer@uci.edu. .

INTRODUCTION

Ovarian cancer is the fifth leading cause of cancer-related death among women (1, 2). Ninety-percent of malignant ovarian cancers are epithelial and are thought to originate from the ovarian surface epithelium, the fallopian tube epithelium or the uterine epithelium, while 7% are sex cord stromal tumors such as granulosa cell tumors and thecomas (3, 4). Risk of ovarian cancer increases with higher number of lifetime ovulations. Thus, pregnancies, breast-feeding and hormonal contraceptive use, which reduce the lifetime number of ovulatory cycles, are associated with reduced risk of ovarian cancer (5–7). Among environmental exposures, tobacco smoking and ionizing radiation exposure are associated with increased risk of ovarian cancer (6–9). Experimental studies show that the ovary is highly susceptible to ionizing radiation-induced tumors. Irradiation of adult mice with high-dose rates of low-linear energy transfer (LET) gamma rays, X rays or protons causes ovarian tumors with maximum prevalence of 40–60% at doses of 0.5 to 1.5 Gy (10, 11). Consistent with these data in mice, female survivors of the atomic bombs in Japan had increased incidence of ovarian cancer (12, 13).

During deep space missions, astronauts are exposed to solar particle events (SPE) and galactic cosmic rays (GCR). SPE are composed of 90% protons and 10% other ions. GCR contain a mixture of ions including 1% ions heavier than helium, known as high-charge and energy (HZE) particles (14). HZE particles have high LET and produce ionization densely along their paths (15, 16). Approximately 21% of the ionizing radiation dose equivalent of GCR to astronauts in a spacecraft is estimated to come from HZE particles, with 2% coming from iron alone (17). It is estimated that astronauts will be exposed to 40 cGy absorbed dose of ionizing radiation during a three-year Mars mission (18). Women made up one-half of the 2013 National Aeronautics and Space Administration (NASA) astronaut class (19), but very few studies been done to investigate the effects of cosmic radiation on the ovary. We recently showed that charged-iron and oxygen particles are highly damaging to the ovary even at low doses, causing premature ovarian failure (20, 21). Although destruction of ovarian germ cells by ionizing radiation, chemical toxicants and other experimental manipulations is associated with subsequent development of ovarian tumors (22–24), there have been very few studies of ovarian tumor induction by HZE particles. Irradiation of female mice with 43.9 cGy of 290 MeV/u carbon ions (LET 10 keV/μm) increased the incidence of ovarian tumors to 23% from 0% in controls (25), while 20 cGy of 1 GeV iron ions (LET 148 keV/μm) increased the incidence of ovarian tumors to 8% from 3% in controls (26). In neither of these studies was any molecular characterization performed on the ovarian tumors that were observed. This constitutes an important data gap, which we addressed in the current study.

We hypothesized that charged-iron-particle irradiation induces epithelial ovarian tumors originating in the ovarian surface epithelial cells. We performed detailed histopathological and immunohistochemical analyses of ovaries of irradiated and control mice 15 months postirradiation.

MATERIALS AND METHODS

Animals

Twelve-week-old C57BL/6J female mice (N = 15/treatment group; Jackson Laboratory, Bar Harbor, ME) were exposed to 0 (sham) or 50 cGy charged-iron particles (LET = 179 keV/μm) at energy of 600 MeV/u and dose rates of 13.5–18.6 cGy/min. The fluence was 1.835×10^6 particles/cm^2. This translates to approximately 0.9 cell traversals for an ovarian surface epithelial cell (area ≈ 50 μm^2) and approximately 1.8 traversals for a primordial follicle oocyte (area ≈ 113 μm^2). Irradiations were performed at the NASA Space Radiation Laboratory, Brookhaven National Laboratory (Upton, NY) (27). Sham-irradiated mice were transported and restrained in the same manner and for the same duration of time as irradiated mice. After irradiation, mice were shipped to and followed for 15 months at the University of California Irvine (UC Irvine) vivarium. Mice were monitored for palpable tumors twice weekly and weighed biweekly initially and weekly after 54 weeks of age. Mice that showed significant (≥10%) weight loss or palpable tumors larger than 1 cm were sacrificed immediately, instead of at the planned 15-month necropsy time point. Ovaries with attached oviducts were harvested and fixed in Bouin's fixative (Thermo Fisher Scientific™ Inc., Waltham, MA) or in 4% paraformaldehyde (Electron Microscopy Sciences) in phosphate buffered saline. All animal procedures were approved by the Institutional Animal Care and Use Committees (IACUC) at both Brookhaven National Laboratory and UC Irvine.

Vaginal Cytology

To evaluate radiation-related changes in estrous cycles, microscopic examination of fresh vaginal lavage fluid obtained in 0.9% sodium chloride (28) was performed for five mice from each group every morning beginning at 12 months postirradiation and continuing for three estrous cycles or day 14 if the mice were not cycling. Mice were housed individually for one week before and while monitoring estrous cycles. To avoid potential estrous cycle-related differences in ovarian end points, vaginal cytology was also performed prior to necropsy at 15 months postirradiation; mice were euthanized on the first day with leukocytic vaginal cytology.

Ovarian Histomorphometric Analysis

Bouin's-fixed ovaries were paraffin embedded and serially sectioned at 5 μm thickness. Paraformaldehyde-fixed ovaries were embedded in Tissue-Tek® optimum cutting temperature (OCT) compound (Electron Microscopy Sciences, Hatfield, PA), stored at −80°C and serially cryosectioned at 10 μm thickness. Every tenth serial section was H&E stained with Gill's hematoxylin (Thermo Fisher Scientific) and 1% eosin Y (Sigma-Aldrich). Ovarian sections were examined for abnormalities using light microscopy blind to treatment group by two of the authors, one of whom (GWL) is a board-certified veterinary pathologist. Two perpendicular tumor diameters were measured in the largest tumor cross-section using a calibrated ocular micrometer, and the average of the diameters was used for comparison of tumor size by radiation dose.

Immunohistochemical Analysis

Bouin's-fixed or paraformaldehyde-fixed sections were subjected to antigen retrieval using 10 mmol/l sodium citrate with 0.05% Tween™ 20 at 95°C, blocked with avidin, biotin blocking reagents and normal goat serum (all from Vector® Laboratories, Burlingame, CA), and incubated with primary antibodies directed against cytokeratin, Ki67, ALDH1 or FOXL2 and secondary antibody, as detailed in Table 1. Sections were then blocked with 0.3% H_2O_2 and incubated with ABC reagent (Vector Laboratories). Immunostaining was visualized with diaminobenzidine substrate in peroxide buffer (Roche Diagnostics, Indianapolis, IN). Sections were lightly counterstained with hematoxylin. The following negative controls were included in each immunostaining run: 1. primary antibody without secondary antibody; 2. primary antibody replaced by nonimmune IgG with secondary antibody; 3. secondary antibody without primary antibody. Additional controls included ovarian sections from 8-week-old 50 cGy iron-ions irradiated mice from our previously published study (21). Scoring of immunostaining was done without knowledge of the treatment groups. Ki67 and FOXL2 immunostaining were only performed on five ovaries per treatment group that had been fixed in paraformaldehyde because Bouin's fixation apparently destroyed or masked the epitope to which these antibodies bind. Cytokeratin and ALDH1 immunostaining were performed using both Bouin's-fixed and paraformaldehyde-fixed ovaries.

The numbers of Ki67 immunopositive and immunonegative cells were counted blind to treatment group in three random 100 × 100 μm fields in three separate sections per each of five ovaries per treatment group. In ovaries with ovarian follicles, only random fields that did not contain follicles were counted. The mean percentage of positive cells per ovary was then calculated.

Statistical Analyses

The effect of radiation on body weight over time postirradiation was analyzed using generalized estimating equations (GEE), a form of general linear model, to adjust for repeated measures within animals. Differences between groups in the number of mice cycling and number with tumors were analyzed using Fisher's exact test. Difference in tumor multiplicity between groups was analyzed using Somers' D test. Maximum tumor diameter in each group was expressed as mean ± standard deviation, and diameters were compared using independent samples *t* test. The effect of radiation on the percentage of estrous cycle days with leukocytic vaginal cytology was analyzed by Mann-Whitney nonparametric test.

RESULTS

Charged-Iron-Particle Irradiation Increase Body Weight Gain and Disrupt Estrous Cycling

After irradiation, body weight was monitored biweekly. Mice irradiated with 50 cGy iron showed a clear, though not statistically significant, trend of greater weight gain over time compared to control mice (Fig. 1; $P = 0.06$, effect of radiation on body weight, GEE). Estrous cycling was evaluated by vaginal cytology in a subset of five mice per group at 12 months postirradiation. All of the irradiated mice were acyclic, while 3 of 5 control mice

cycled, albeit irregularly ($P = 0.17$, Fisher's exact test). Irradiated mice had predominantly leukocytic vaginal cytology, consistent with metestrus or diestrus, on 97 ± 3% of days, while control mice had leukocytic cytology 62 ± 10% of days ($P = 0.013$, Mann-Whitney test).

Charged-Iron-Particle Irradiation Induced Ovarian Tumors

Examination of every tenth ovarian serial section at 15 months postirradiation revealed that 20% of the control mice had a few growing follicles and corpora lutea in the ovaries, consistent with continued estrous cycling in some of these mice (Fig. 2A). Follicles and corpora lutea were completely absent in irradiated mice (Fig. 2B–D). Invagination of the ovarian surface epithelium was observed in irradiated mice. Ovaries of irradiated mice without tumors also showed occasional tubular structures (Fig. 2B), which are very similar to the much more numerous tubules observed in the ovarian tumors (Fig. 2C and D). Of the irradiated mice, 47% had unilateral ovarian tumors, which were diagnosed as tubular adenomas, and 7% had bilateral tubular adenomas (Fig. 2C and D), while only 14% of control mice had unilateral and none had bilateral ovarian tubular adenomas ($P < 0.04$, Fisher's exact test for presence of tubular adenomas and Somers' D test for tumor multiplicity). No oviductal tumors were noted. In addition to being more numerous, the tumors tended to be larger in the irradiated mice. The average tumor diameter in the largest cross-section was 1,000 ± 283 μm in the two controls and 1,996 ± 875 μm in the eight irradiated mice with tumors ($P = 0.034$, *t* test).

On gross inspection at necropsy, abnormalities were noted in other organs (uterus, spleen, liver, lymph nodes, lung, kidney, pancreas), but there was no difference in the prevalence of any of these gross abnormalities between irradiated and control mice. The highest prevalence of 36% was noted for spleen abnormalities (increased size and/or nodules) in controls.

Charged-Iron-Particle-Radiation-Induced Ovarian Tumors were Epithelial

To further confirm the histopathological diagnosis of tubular adenoma, an epithelial tumor, we performed immunostaining using a pan-cytokeratin antibody (Fig. 3). At 15 months postirradiation, cells lining the tubular structures in nontumor-bearing ovaries and lining the tubules of the tubular adenomas were cytokeratin positive, confirming that these were epithelial tumors (Fig. 3A–C). As expected, in sham-irradiated control mice only the single layer of ovarian surface epithelial cells was cytokeratin positive (Fig. 3D). At 8 weeks after 50 cGy iron-ion irradiation, ovaries were essentially devoid of follicles (21), and only ovarian surface epithelial cells were immunopositive for cytokeratin (Fig. 3E). We also analyzed proliferation using Ki67 immunostaining in a subset of ovaries (Fig. 4). In control ovaries (N = 5), Ki67 immunostaining was observed in most granulosa cells of growing follicles (Fig 4C), but in very few cells in the ovarian stroma (1.2 ± 0.8% positive stromal cells/total number of cells). In irradiated ovaries (Fig. 4A and B; N = 5) with or without tubular adenomas, there were few Ki67 positive cells (1.1 ± 0.5% positive cells/total number of cells). Moreover, consistent with low Ki67 staining, very few mitotic figures were noted in the ovarian tumors.

ALDH1-positive epithelial cells at the junction of the ovarian surface epithelium, mesothelium and oviductal epithelium (the ovarian hilum) have been reported to constitute a cancer-prone stem cell niche from which epithelial ovarian tumors may arise (29). Therefore, we performed immunostaining for ALDH1. We observed ALDH1 immunopositivity throughout the ovarian stroma and in surface epithelial cells at the hilum, as well as throughout the ovarian surface epithelium, but not in granulosa cells in control ovaries from mice sacrificed at 15 months (Fig. 5A) and 8 weeks (Fig. 5B) postirradiation. We also observed ALDH1 staining in the ovarian tumors in irradiated mice. Interestingly, ALDH1 staining was observed in the cytokeratin-positive cells lining the tubules, as well as in some tumor areas that were negative for cytokeratin (compare Fig. 3A–C with Fig. 5C–F).

To determine whether the tumors contained granulosa cell tumor components, we performed immunostaining with a FOXL2 antibody in a subset of ovaries (Fig. 6). FOXL2 is a granulosa cell marker used to diagnose granulosa cell ovarian tumors (30). As expected, FOXL2 immunostaining was detected in the granulosa cells of growing follicles, but very rarely in the ovarian stroma, of sham-irradiated mice (N = 5; Fig. 6A). FOXL2 immunostaining was not detected in the cytokeratin-positive epithelial cells lining the tubular structures within an ovarian tumor of an irradiated mouse, but was detected in clusters of cells between the tubules that were granulosa cell-like in appearance (Fig. 6B and C). A similar cluster of FOXL2-positive cells was observed in a nontumor-bearing ovary of an irradiated mouse (data not shown). Thus, we concluded that some of the ovarian tumors we observed in irradiated mice were mixed tubular adenoma/granulosa cell tumors.

DISCUSSION

We observed a nearly fourfold increase in ovarian tumor prevalence at 15 months after 50 cGy charged-iron-particle irradiation compared to sham irradiation. Ovarian tumors in irradiated mice were also larger than those found in controls. The tumor-bearing ovaries were devoid of follicles, and the tumors were diagnosed as tubular adenomas or mixed tubular adenomas/granulosa cell tumors based on their histology, positive immunostaining for the epithelial marker cytokeratin (31), positive immunostaining for the granulosa cell marker FOXL2 and low numbers of proliferating cells. To our knowledge, this is the first study to report on the immunopathological characterization of ovarian tumors induced by charged-iron particles.

Ninety-percent of malignant ovarian tumors in women are epithelial (32). Thus, it is relevant that the tumors induced by charged-iron particles were epithelial tumors, albeit nonmalignant. Similar to epithelial ovarian cancer in humans, which occurs predominantly in postmenopausal women, tubular adenomas have been shown to occur in multiple experimental rodent models in which ovarian follicle depletion is induced, for example, by ionizing radiation, chemical ovotoxicants, genetic manipulation or other means (22–24), as well as in very old animals (33). On the other hand, tubular adenomas rarely metastasize and do not grow very rapidly. We observed few mitotic figures and few Ki67-positive cells in these tumors, consistent with the nonmalignant nature of tubular adenomas. Thus, tubular adenomas are more similar to human type I epithelial ovarian tumors, which include low-grade serous, endometrioid, clear cell and mucinous carcinomas, than they are to human

type II epithelial ovarian tumors, which include high-grade serous carcinoma, carcinosarcoma and undifferentiated carcinoma (34).

In previously published studies, ALDH1 has been proposed as a marker of ovarian surface epithelial stem cells localized to the hilum (junction between ovarian surface epithelium, ovarian ligament epithelium and oviductal epithelium) by one group (29), while another group (35) reported that ALDH1 was expressed throughout the ovarian surface epithelium. Our results in controls concur with the latter findings. Moreover, to our knowledge, this is the first reported study of ALDH1 expression in ovarian tubular adenomas. Our observations of high levels of ALDH1 protein in stromal cells and tubular adenoma cells are consistent with the previously published finding that ALDH1 is expressed in both stromal cells and tumor cells in human ovaries, with greater expression in tumor cells associated with well-differentiated tumors that have a better prognosis (36).

In general, the potency of 50 cGy iron ions for ovarian tumor induction in the current study appears to be higher than similar doses of gamma rays or protons. However, comparisons among studies are limited by the lack of side-by-side comparison of a range of doses of iron ions with photon radiation or protons, as well as by other experimental differences, such as different mouse strains used and different ages at the time of irradiation. The overall ovarian tumor prevalence of 54% is in the range reported for 50 cGy of low-LET X rays (73% at 50 cGy reported by Watanabe *et al.* and 47% at 50 cGy reported by Clapp), but higher than ovarian tumor prevalence reported for similar doses of gamma rays (25% at 50 cGy, reported by Upton *et al.*) and protons (17% at 43 cGy reported by Watanabe *et al.* and 47% at 50 cGy reported by Clapp) (10, 11, 37). The ovarian tumor prevalence of 54% observed in the current study after 50 cGy charged-iron-particle irradiation is higher than the 8% prevalence reported for 20 cGy iron particles (LET 150 keV/μm) in BALB/cByJ mice (26) and higher than the 23% prevalence reported for 44 cGy carbon ions (LET 10 keV/μm) in B6C3F1 mice (25). However, due to the lack of dose-response data within studies and the experimental differences noted above, it is not possible to draw definitive conclusions about relative potencies for ovarian tumorigenesis of various charged particles, gamma rays and X rays.

We observed a borderline significant trend for greater body weight gain over time in iron-ion-irradiated mice compared to sham controls. A similar effect of increased weight gain beginning at approximately 150 days postirradiation was previously reported in carbon-ion-irradiated female mice, but not male mice (25). Continuous exposure to low-dose-rate gamma radiation caused weight gain in male and female B6C3F1 mice, but males gained less weight than females (38). Increased weight gain on a high-fat diet was reported in mice exposed to the ovarian toxicant 4-vinylcyclohexene diepoxide, which also depletes ovarian follicles and causes premature ovarian failure and ovarian tumors (39, 40). The increased weight gain is likely caused by greatly diminished ovarian estrogen production due to ovarian failure. Although we did not measure circulating estradiol concentrations, we have previously shown that by 8 weeks after 50 cGy iron-ion irradiation almost no ovarian follicles remain and circulating luteinizing hormone (LH) and follicle stimulating hormone (FSH) concentrations are significantly elevated, consistent with loss of ovarian negative feedback due to lack of ovarian estrogen production (21). Postmenopausal weight gain with increased central adiposity is observed in women, and perimenopausal estrogen replacement

prevents the increase in central adiposity (41). Androgen deprivation therapy for prostate cancer in men is also associated with weight gain (42).

Elevated concentrations of LH and FSH in postmenopausal women have been postulated to play a role in the pathogenesis of ovarian tumors (43). Various animal models in which ovarian follicles are depleted, resulting in elevated LH and FSH concentrations, develop ovarian tumors (22, 23, 43). More direct evidence for a pathogenic role of high LH and FSH concentrations comes from experiments showing that hypogonadal mice, which have a defect in gonadotropin releasing hormone production and therefore do not produce LH and FSH, do not develop ovarian tumors after irradiation (44). Conversely, suppression of LH and FSH secretion prevents ovarian tumorigenesis in W^xW^v mice, which are genetically deficient in ovarian follicles, have high serum LH and FSH concentrations due to lack of ovarian negative feedback and spontaneously develop ovarian tubular adenomas (45).

In conclusion, our results show that irradiation of adult mice, using charged-iron particles such as those found in galactic cosmic rays, leads to a high prevalence of tubular adenomas and mixed tubular adenoma/granulosa cell ovarian tumors later in life. The tubular adenomas are cytokeratin and ALDH1 positive, consistent with origination from the ovarian surface epithelial cells, which are also considered to be one of the likely cells of origin of epithelial ovarian cancers in humans. Our results raise concerns about the development of ovarian cancer as a possible late adverse sequela in women traveling in deep space.

ACKNOWLEDGMENTS

This work was supported by NASA (grant no. NNX14AC50G) and National Institutes of Health (NIH grant nos. R01ES020454 to UL and P30CA062203), the University of California Irvine (UC Irvine) Chao Family Comprehensive Cancer Center. Additional support was provided by the UC Irvine, CCenter for Occupational and Environmental Health and Summer Undergraduate Research Program fellowship to RR. In addition, BM was partially supported by a First award fellowship from the National Space Biomedical Research Institute (grant no. PF04302). We thank Drs. Peter Guida, Chiara La Tessa, Adam Rusek and the NASA Space Radiation Laboratory staff for their support.

REFERENCES

1. Romero I, Bast RC. Minireview: Human ovarian cancer: biology, current management, and paths to personalizing therapy. Endocrinology 2012; 153:1593–602. [PubMed: 22416079]
2. Chen VW, Ruiz B, Killeen JL, Cote TR, Wu XC, Correa CN. Pathology and classification of ovarian tumors. Cancer 2003; 97:2631–42. [PubMed: 12733128]
3. Mullany LK, Richards JS. Minireview: Animal models and mechanisms of ovarian cancer development. Endocrinology 2012; 153:1585–92. [PubMed: 22396450]
4. Kurman RJ, Shih I-M. The origin and pathogenesis of epithelial ovarian cancer: A proposed unifying theory. Am J Surg Pathol 2010; 34:433–43. [PubMed: 20154587]
5. Whittemore AS, Harris R, Itnyre J, COC Group. Characteristics relating to ovarian cancer risk: Collaborative analysis of 12 US case-control studies. IV. The pathogenesis of epithelial ovarian cancer. Am J Epidemiol 1992; 136:1212–19. [PubMed: 1476143]
6. Gates MA, Rosner BA, Hecht JL, Tworoger SS. Risk factors for epithelial ovarian cancer by histologic subtype. Am J Epidemiol 2010; 171:45–53. [PubMed: 19910378]
7. Kurian AW, Balise RR, McGuire V, Whittemore AS. Histologic types of epithelial ovarian cancer: Have they different risk factors? Gynecol Oncol 2005; 96:520–30. [PubMed: 15661246]

8. Travis LB, Ng AK, Allan JM, Pui C-H, Kennedy AR, Xu XG, et al. Second malignant neoplasms and cardiovascular disease following radiotherapy. J Natl Cancer Inst 2012; 104:357–70. [PubMed: 22312134]
9. Hodgson DC, Gilbert ES, Dores GM, Schonfeld SJ, Lynch CF, Storm H, et al. Long-term solid cancer risk among 5-year survivors of Hodgkin's lymphoma. J Clin Oncol 2007; 25:1489–97. [PubMed: 17372278]
10. Clapp NK. Ovarian tumor types and their incidence in intact mice following whole body exposure to ionizing radiation. Radiat Res 1978; 74:405–15. [PubMed: 684159]
11. Upton AC, Randolph ML, Conklin JW. Late effects of fast neutrons and gamma rays in mice as influenced by the dose rate of irradiation: induction of neoplasia. Radiat Res 1970; 41:467–91. [PubMed: 4908840]
12. Inai K, Shimizu K, Kawai K, Tokunaga M, Soda M, Mabuchi K, et al. A pathology study of malignant and benign ovarian tumors among atomic bomb survivors. J Radiat Res (Tokyo) 2006; 47:49–59. [PubMed: 16571918]
13. Tokuoka S, Kawai K, Shimizu Y, Inai K, Ohe K, Fujikura T, et al. Malignant and benign ovarian neoplasms among atomic bomb survivors, Hiroshima and Nagasaki, 1950–80. J Natl Cancer Inst 1987; 79:47–57. [PubMed: 3474449]
14. Bourdarie S, Xapsos M. The near-earth space radiation environment. IEEE Trans Nucl Sci 2008; 55:1810–32.
15. Tokuyama Y, Furusawa Y, Ide H, Yasui A, Terato H. Role of isolated and clustered DNA damage and the post-irradiating repair process in the effects of heavy ion beam irradiation. J Radiat Res (Tokyo) 2015; 56:446–55. [PubMed: 25717060]
16. Sridharan DM, Asaithamby A, Bailey SM, Costes SV, Doetsch PW, Dynan WS, et al. Understanding cancer development processes after HZE-particle exposure: Role of ROS, DNA damage repair and inflammation. Radiat Res 2015; 183:1–26. [PubMed: 25564719]
17. Slaba TC, Blattnig SR, Norbury JW, Rusek A, La Tessa C, Walker SA. GCR simulator reference field and a spectral approach for laboratory simulation. NASA Technical Publication, NASA/TP-2015-218698; Langley, VA: NASA; 2015.
18. Cucinotta FA. Durante M. Cancer risk from exposure to galactic cosmic rays: Implications for space exploration by human beings. Lancet Oncol 2006; 7:431–35. [PubMed: 16648048]
19. Ronca AE, Baker ES, Bavendam TG, Beck KD, Miller VM, Tash JS, et al. Effects of sex and gender on adaptations to space: Reproductive health. J Womens Health 2014; 23:967–74.
20. Mishra B, Ripperdan R, Ortiz L, Luderer U. Very low doses of heavy oxygen ion radiation induce premature ovarian failure. Reproduction 2017; 154:123–33. [PubMed: 28528322]
21. Mishra B, Ortiz L, Luderer U. Charged iron particles, typical of space radiation, destroy ovarian follicles. Hum Reprod 2016; 31:1816–26. [PubMed: 27251203]
22. Vanderhyden BC, Shaw TJ, Ethier J-F. Animal models of ovarian cancer. Repro Biol Endocrinol 2003; 1:67.
23. Capen CC, Beamer WG, Tennent BJ, Stitzel KA. Mechanisms of hormone-mediated carcinogenesis in the ovary of mice. Mutat Res 1995; 333:143–51. [PubMed: 8538621]
24. Lim J, Lawson GW, Nakamura BN, Ortiz L, Hur JA, Kavanagh TJ, et al. Glutathione-deficient mice have increased sensitivity to transplacental benzo[a]pyrene-induced premature ovarian failure and ovarian tumorigenesis. Cancer Res 2013; 73:908–17. [PubMed: 23135907]
25. Watanabe H, Ogiu T, Nishizaki M, Fujumoto N, Kido S, Ishimura Y, et al. Induction of ovarian tumors by heavy ion irradiation in B6C3F1 mice. Oncol Rep 1998; 5:1377–80. [PubMed: 9769371]
26. Bielefeldt-Ohmann H, Genik PC, Fallgren CM, Ullrich RL, Weil MM. Animal studies of charged particle-induced carcinogenesis. Health Phys 2012; 103:568–76. [PubMed: 23032886]
27. La Tessa C, Sivertz M, Chiang I-H, Lowenstein D, Rusek A. Overview of the NASA Space Radiation Laboratory. Life Sci Space Res 2016; 11:18–23.
28. Cooper RL, Goldman JM, Vandenbergh JG. Monitoring of the estrous cycle in the laboratory rodent by vaginal lavage. In: Heindel JJ, Chapin RE, editors. Female reproductive toxicology. San Diego: Academic Press, Inc; 1993.

29. Flesken-Nikitin A, Hwang C-I, Cheng C-Y, Michurina TV, Enikolopov G, Nikitin AY. Ovarian surface epithelium at the junction area contains a cancer-prone stem cell niche. Nature 2013; 495:241–45. [PubMed: 23467088]
30. Al-Agha OM, Huwait HF, Chow C, Yang W, Senz J, Kalloger SE, et al. FOXL2 Is a sensitive and specific marker for sex cord-stromal tumors of the ovary. Am J Surg Pathol 2011; 35:484–94. [PubMed: 21378549]
31. Yang W-L, Cai KQ, Smedberg JL, Smith ER, Klein-Szanto A, Hamilton TC, et al. A reduction of cyclooxygenase 2 gene dosage counters the ovarian morphological aging and tumor phenotype in Wv mice. Am J Pathol 2007; 170:1325–36. [PubMed: 17392171]
32. Vanderhyden BC, Shaw TJ, Garson K, Tonary AM. Ovarian carcinogenesis. In: Leung PCK, Adashi EY, editors. The ovary. San Diego: Elsevier Academic Press; 2004.
33. Engle ET. Tubular adenomas and testis-like tubules of the ovaries of aged rats. Cancer Res 1946; 6:578–82. [PubMed: 20996758]
34. Kurman RJ, Shih I-M. The dualistic model of ovarian carcinogenesis. revisited, revised, and expanded. Am J Pathol 2016; 186:733–47. [PubMed: 27012190]
35. Ng A, Tan S, Singh G, Rizk P, Swathi Y, Tan TZ, et al. Lgr5 marks stem/progenitor cells in ovary and tubal epithelia. Nat Cell Biol 2014; 16:745–57. [PubMed: 24997521]
36. Humag R, Li X, Holm R, Trope CG, Nesland JM, Suo Z. The expression of aldehyde dehydrogenase 1 (ALDH1) in ovarian carcinomas and its clinicopathological associations: A retrospecitive study. BMC Cancer 2015; 15:502. [PubMed: 26148881]
37. Watanabe H, Ogiu T, Nishimura N, Masaoka Y, Kurosumi M, Takahashi T, et al. Comparison of tumorigenesis between accelerated heavy ion and X-ray in B6C3F1 mice. J Radiat Res (Tokyo) 1998; 39:93–100. [PubMed: 9735597]
38. Tanaka IB, Tanaka S, Ichinohe K, Matsushita S, Matsumoto T, Otsu H, et al. Cause of death and neoplasia in mice continuously exposed to very low dose rates of gamma rays. Radiat Res 2007; 167:417–37. [PubMed: 17388697]
39. Romero-Aleshire MJ, Diamond-Stanic MK, Hasty AH, Hoyer PB, Brooks HL. Loss of ovarian function in the VCD mouse-model of menopause leads to insulin resistance and a rapid progression into the metabolic syndrome. Am J Physiol 2009; 297:R587–92.
40. NTP. NTP technical report on the toxicology and carcinogenesis studies of 4-vinyl-1-cyclohexene diepoxide (CAS No. 106-87-6) in F344/N Rats and B6C3F1 Mice (Dermal Studies). Report No. NTP TR 362 Research Triangle Park, NC: National Toxicology Program, U.S. Department of Health and Human Services, Public Health Service, National Institutes of Health; 1989.
41. Kapoor E, Collazo-Clavell ML, Faubion SS. Weight gain in women at midlife: A concise review of the pathophysiology and strategies for management. Mayo Clin Proc 2017; 92:1552–58. [PubMed: 28982486]
42. Urushima H, Inomata-Kurashiki Y, Nishimura K, Sumi R, Shimomura I, Nonomura N, et al. The effects of androgen deprivation therapy with weight management on serum aP2 and adiponectin levels in prostate cancer patients. The Aging Male 2015; 18:72–76. [PubMed: 25746209]
43. Salehi F, Dunfield L, Phillips KP, Krewski D, Vanderhyden BC. Risk factors for ovarian cancer: An overview with emphasis on hormonal factors. J Toxicol Environ Health B Crit Rev 2008; 11:301–21. [PubMed: 18368558]
44. Tennent BJ, Beamer WG. Ovarian tumors not induced by irradiation and gonadotropins in hypogonadal (hpg) mice. Biol Reprod 1986; 34:751–60. [PubMed: 3708055]
45. Blaakaer J, Baeksted M, Micic S, Albrectsen P, Rygaard J, Bock J. Gonadotropin-releasing hormone agonist suppression of ovarian tumorigenesis in mice of the Wx/Wv genotype. Biol Reprod 1995; 53:775–79. [PubMed: 8547469]

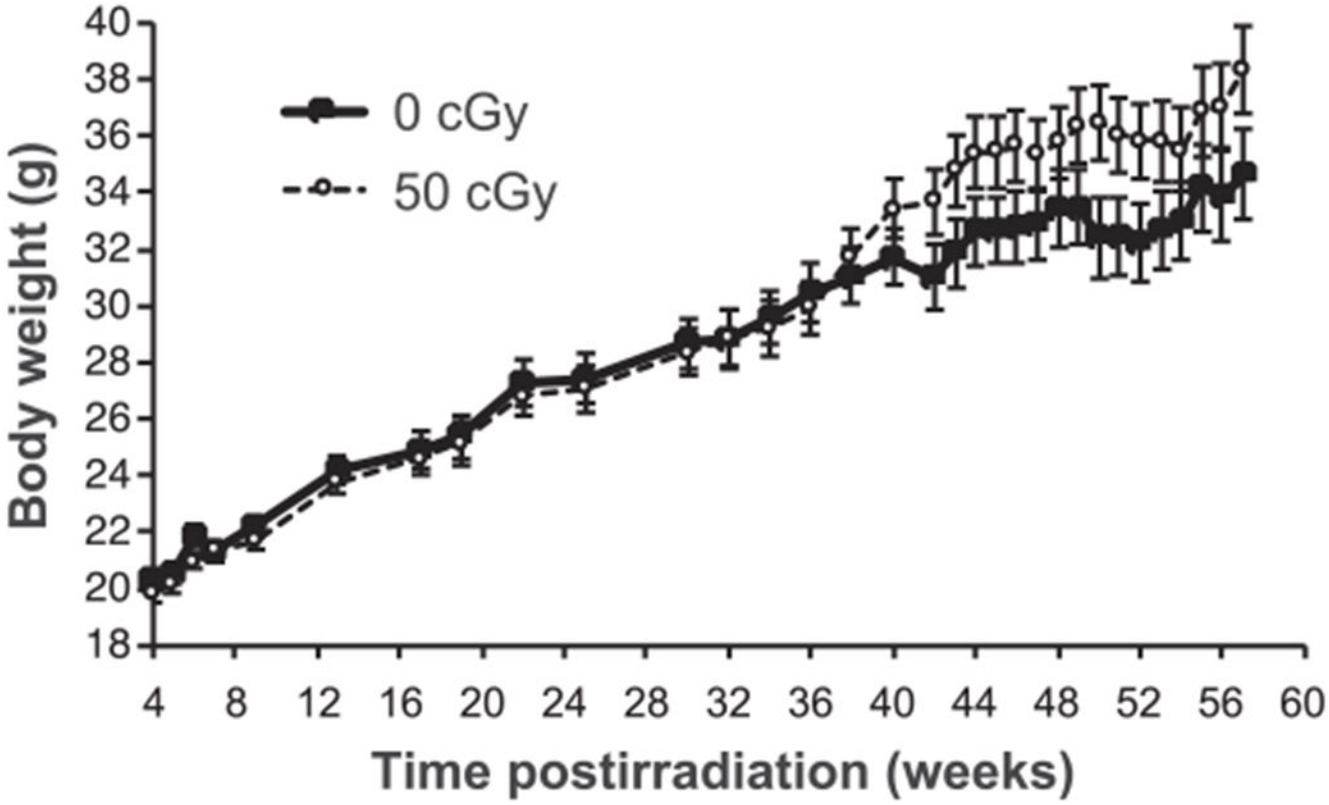

FIG. 1.

Charged-iron-particle irradiation leads to increased weight gain with aging. Graph shows the means ± SEM body weights. Body weight was monitored for up to 15 months after 50 cGy or sham (0 cGy) irradiation at 12 weeks of age. There was a trend towards higher weight gain in the irradiated group beginning 40 weeks postirradiation ($P = 0.06$, effect of radiation on body weight, GEE).

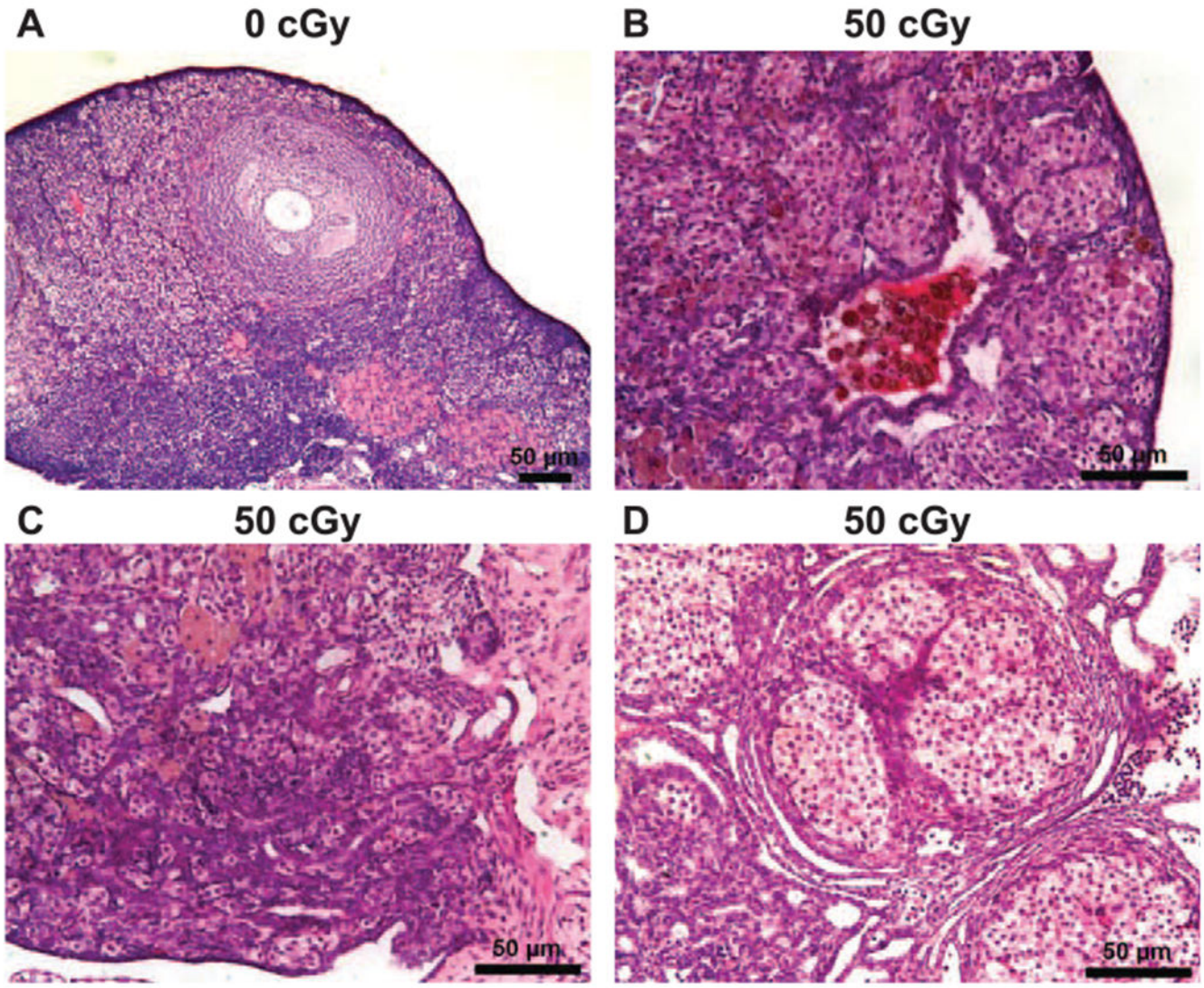

FIG. 2.

Mice irradiated with charged-iron particles develop ovarian tumors. Treatment groups were the same as for Fig. 1, and ovaries were harvested at necropsy 15 months postirradiation. Ovarian sections were H&E stained. Panel A: Ovarian section from 0 cGy control group has antral follicle. Panel B: Tubular structure within nontumor-bearing ovary from 50 cGy iron-irradiated mouse. Panels C and D: Representative ovarian tumor histology from the 50 cGy iron-irradiated group showing tubular structures within the ovarian parenchyma and complete absence of follicles. Tumors were histologically classified as tubular adenomas.

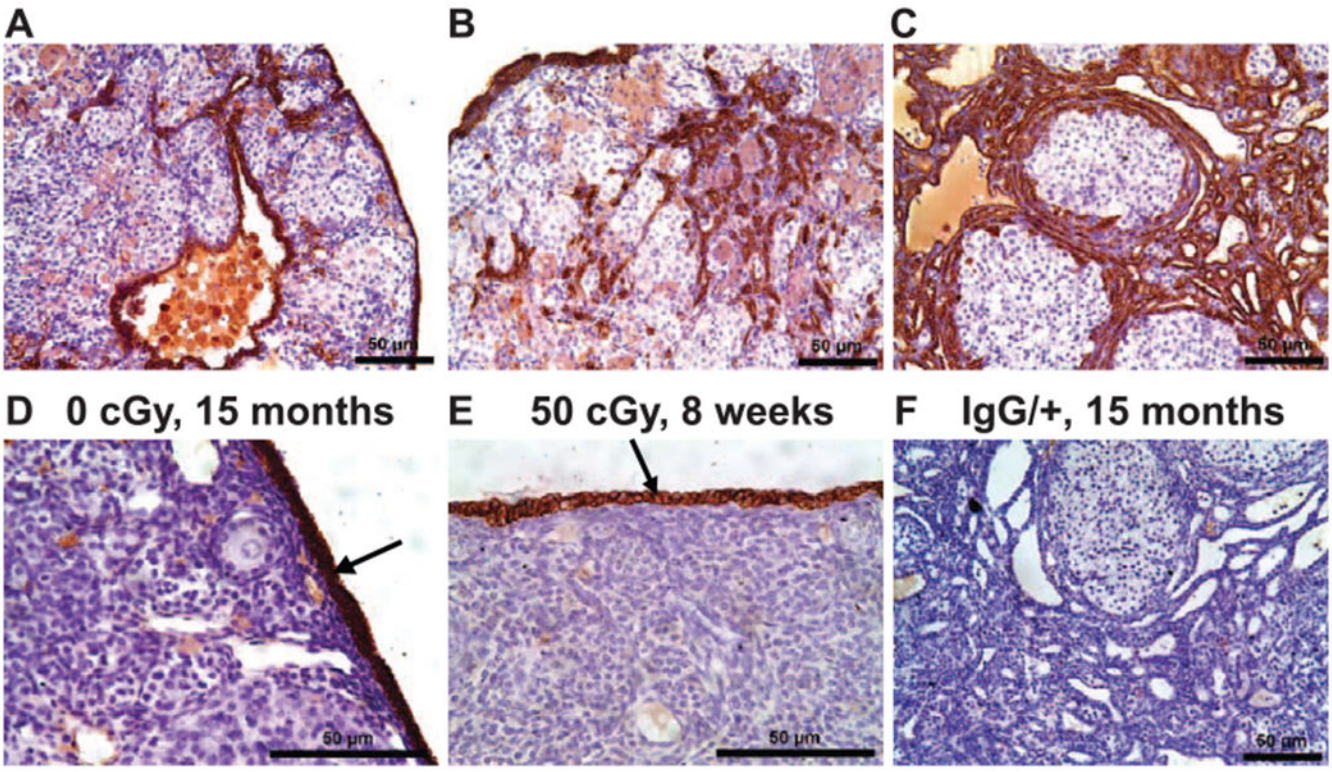

FIG. 3.

Charged-iron-particle-radiation-induced ovarian tumors are positive for the epithelial cell marker cytokeratin. Representative images of cytokeratin immunostaining. Cyst (panel A) and ovarian tumors (panels b and C) tumors from irradiated mice show positive (brown) cytokeratin immunostaining in cells lining tubular structures. Ovary shown in panel A is the same ovary as is shown in Fig. 2B and ovary in panel C is same ovary as in Fig. 2D. Panel D: Section from ovary collected 15 months after sham irradiation has primary follicle and is cytokeratin positive only in ovarian surface epithelial cells (arrow). Panel E: Ovary collected at 8 weeks after 50 cGy charged-iron-particle irradiation shows absence of follicles and cytokeratin immunostaining in ovarian surface epithelial cells (arrow). Panel F: Lack of immunostaining in technical negative control with primary antibody replaced by nonimmune IgG. Scale bars = 50 µm.

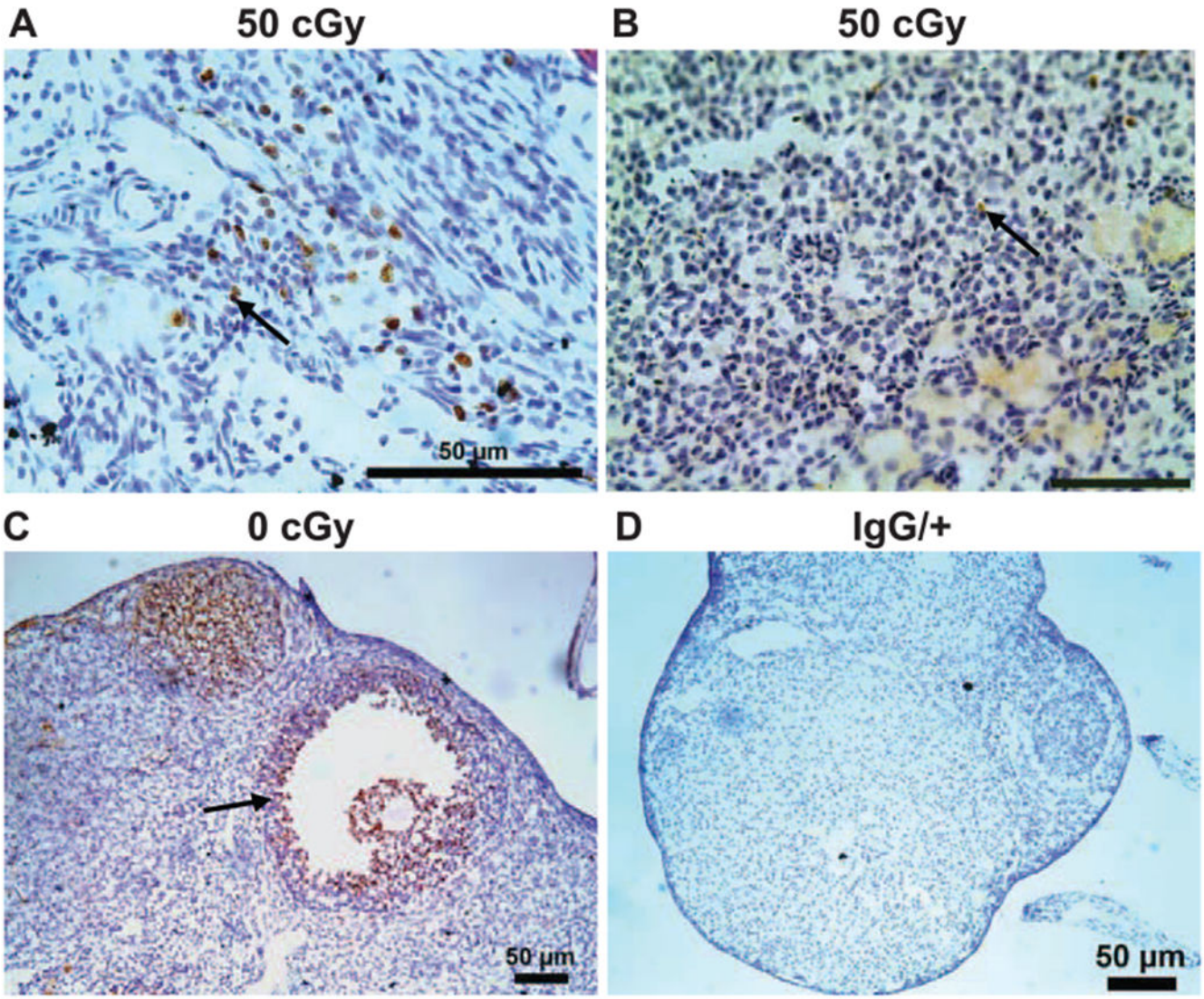

FIG. 4.

Few proliferating cells in ovarian tumors induced by charged-iron-particle irradiation. Representative images of Ki67 immunostaining. Panels A and B: Ovaries from irradiated mice show few Ki67-immunopositive (brown) cells. Panel C: Ovarian sections from control ovary with immunopositive granulosa cells. Panel D: Lack of immunostaining in technical negative control with primary antibody replaced by nonimmune IgG. Scale bars = 50 μm. Black arrows indicate representative immunopositive cells.

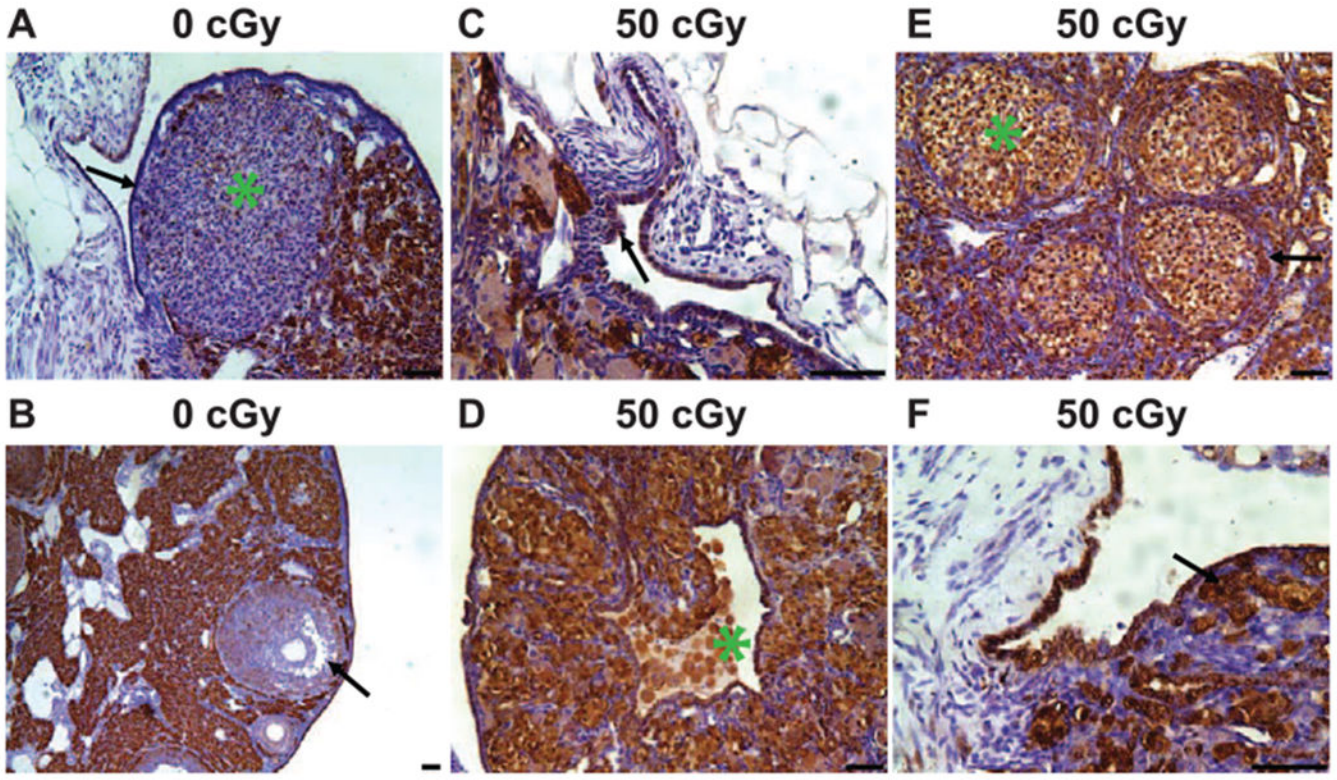

FIG. 5.

ALDH immunostaining in ovaries of control and charged-iron-particle-irradiated mice. Representative images of ALDH1 immunostaining. Panels A and B: Ovaries from 0 cGy control mice aged 15 months and 8 weeks, respectively, with ALDH1-positive (brown stain) in the ovarian surface epithelium (black arrow in panel A), hilar epithelium and stroma, but minimal staining in corpus luteum (green asterisk in panel A) or granulosa cells of follicles (arrow in panel B). Panels C and D: Ovaries from 50 cGy irradiated mice show increased immunostaining at the ovarian surface epithelium and epithelial tubular structure (green asterisk in panel D, compare with Fig. 3A), hilum region (arrow in panel C) and stroma compared to control ovaries. Panels E and F: Ovarian tumors from 50 cGy irradiated mice show immunostaining in the cells lining the tubules, which were positive for cytokeratin (black arrows), and tumor cells that were negative for cytokeratin (green asterisk in panel E, compare with Fig. 3C). Scale bars = 50 μm.

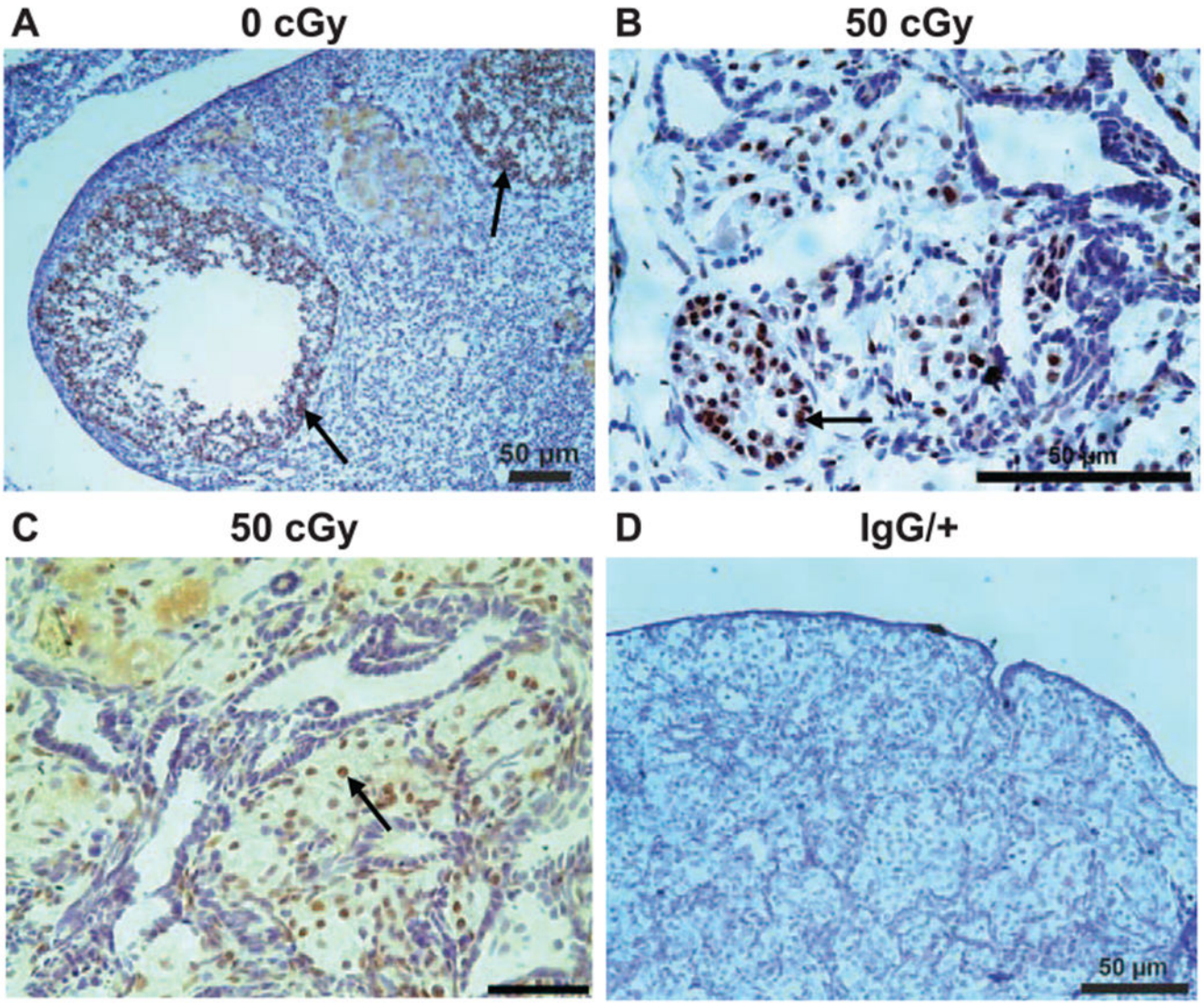

FIG. 6.

Charged-iron-particle-radiation-induced ovarian tumors have granulosa cell components. Representative images of FOXL2 immunostaining. Panel A: Ovary from 0 cGy control mouse with FOXL2-positive (brown) granulosa cells. Panel B: Ovary from 50 cGy irradiated mouse has FOXL2-positive cells in cell packets between tubular structures, but not in tubule epithelial cells. Panel C: Ovary from another 50 cGy irradiated mouse with similar staining pattern as in panel B. Panel D: Lack of FOXL2 immunostaining in technical negative control with primary antibody replaced by nonimmune IgG. Arrows indicate representative immunopositive cells. Scale bars = 50 μm.

TABLE 1

Antibodies Used for Immunohistochemistry

Protein target	Name of antibody	Manufacturer	Species raised in; monoclonal or polyclonal	Primary antibody dilution	Secondary antibody dilution
Cytokeratin	Anti-pancytokeratin	Cell Signaling, 9718	Rabbit; monoclonal	1:100	1:500
ALDH1	Anti-aldehyde dehydrogenase-1A1	Abcam, ab23375	Rabbit, polyclonal	1:500	1:1,000
Ki67	Anti-Ki67	Abcam, ab15580	Rabbit; polyclonal	1:200	1:200
FOXL2	Anti-FOXL2	Abcam, ab5096	Goat; polyclonal	1:500	1:400